Electronic supplementary information (ESI)

Long- and short-range structures of $Ti_{1-x}Hf_xNi_{1.0/1.1}Sn$ half-Heusler compounds and their electric transport properties

Matylda N. Guzik,[a, b,*] Matthias Schrade,[b] Raluca Tofan,[b] Patricia A. Carvalho,[c] Kristian Berland,[b, d] Magnus H. Sørby,[a] Clas Persson,[b] Anette E. Gunnæs,[b] Bjørn C. Hauback[a]

[a]Physics Department, Institute for Energy Technology, P.O. Box 40, N-2027 Kjeller, Norway

[b]Department of Physics, Centre for Materials Science and Nanotechnology, University of Oslo, P.O. Box 1048 Blindern, N-0316 Oslo, Norway

[c]SINTEF Materials and Chemistry, P.O. Box 124 Blindern, N-0314 Oslo, Norway

[d]Faculty of Science and Technology, Norwegian University of Life Sciences, P.O. Box 5003 NMBU, N-1432 Ås, Norway

Corresponding Author

* E-mail: m.n.guzik@its.uio.no

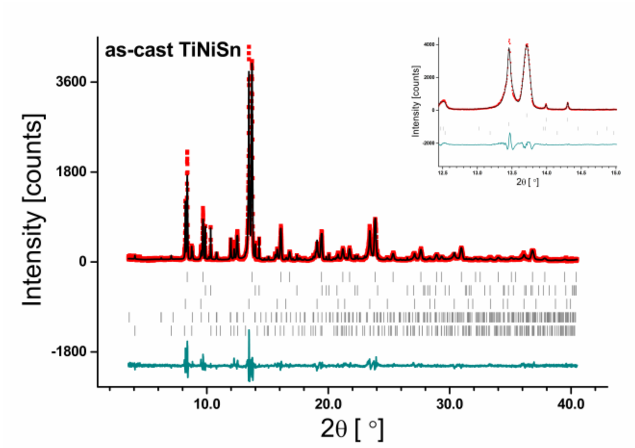

Figure S1. Observed (red), calculated (black) and difference (blue) diffraction profiles collected for as-cast TiNiSn, λ = 0.50218 Å, χ^2 = 2.67. Vertical bars indicate Bragg peak positions of contributing phases, from top to bottom: HH, Sn, FH, Sn_5Ti_6 and Sn_3Ti_5. Inset shows (220) reflections of the HH and FH phases.

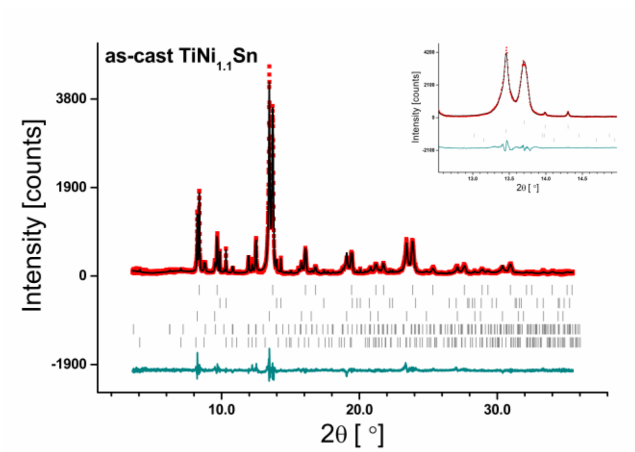

Figure S2. Observed (red), calculated (black) and difference (blue) diffraction profiles collected for as-cast $TiNi_{1.1}Sn$, λ = 0.50218 Å, χ^2 = 2.06. Vertical bars indicate Bragg peak positions of contributing phases, from top to bottom: HH, Sn, FH, Sn_5Ti_6 and Sn_3Ti_5. Inset shows (220) reflections of the HH and FH phases.

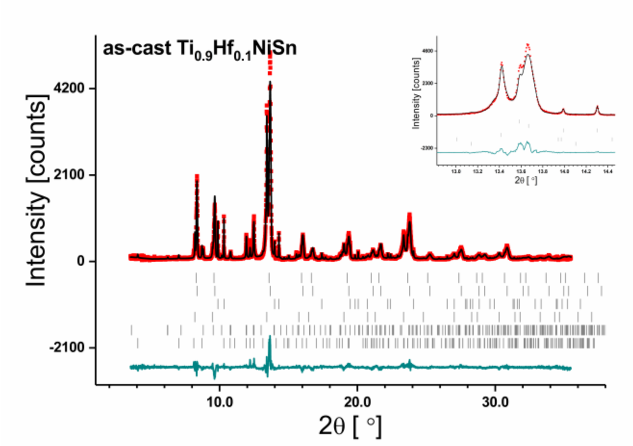

Figure S3. Observed (red), calculated (black) and difference (blue) diffraction profiles collected for as-cast $Ti_{0.9}Hf_{0.1}NiSn$, λ = 0.50218 Å, χ^2 = 2.94. Vertical bars indicate Bragg peak positions of contributing phases, from top to bottom: HH_2, HH_1, Sn, FH, Sn_5Ti_6 and Sn_3Ti_5. Inset shows (220) reflections of the HH and FH phases.

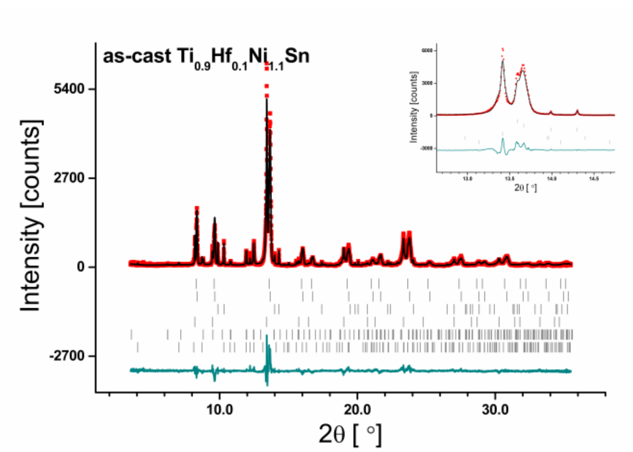

Figure S4. Observed (red), calculated (black) and difference (blue) diffraction profiles collected for as-cast $Ti_{0.9}Hf_{0.1}Ni_{1.1}Sn$, λ = 0.50218 Å, χ^2 = 3.19. Vertical bars indicate Bragg peak positions of contributing phases, from top to bottom HH_2, HH_1, Sn, FH, Sn_5Ti_6 and Sn_3Ti_5. Inset shows (220) reflections of the HH and FH phases.

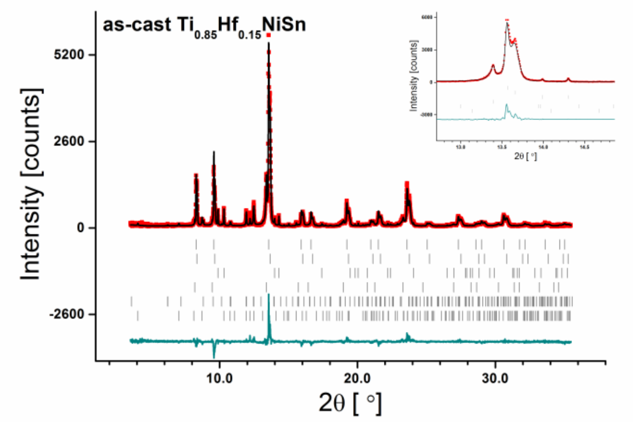

Figure S5. Observed (red), calculated (black) and difference (blue) diffraction profiles collected for as-cast $Ti_{0.85}Hf_{0.15}NiSn$, λ = 0.50218 Å, χ^2 = 2.84. Vertical bars indicate Bragg peak positions of contributing phases, from top to bottom: HH_2, HH_1, Sn, FH, Sn_5Ti_6 and Sn_3Ti_5. Inset shows (220) reflections of the HH and FH phases.

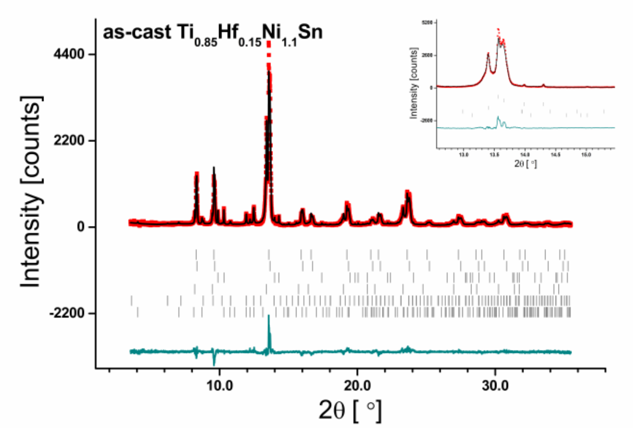

Figure S6. Observed (red), calculated (black) and difference (blue) diffraction profiles collected for as-cast $Ti_{0.85}Hf_{0.15}Ni_{1.1}Sn$, λ = 0.50218 Å, χ^2 = 2.50. Vertical bars indicate Bragg peak positions of contributing phases, from top to bottom: HH_2, HH_1, Sn, FH, Sn_5Ti_6 and Sn_3Ti_5. Inset shows (220) reflections of the HH and FH phases.

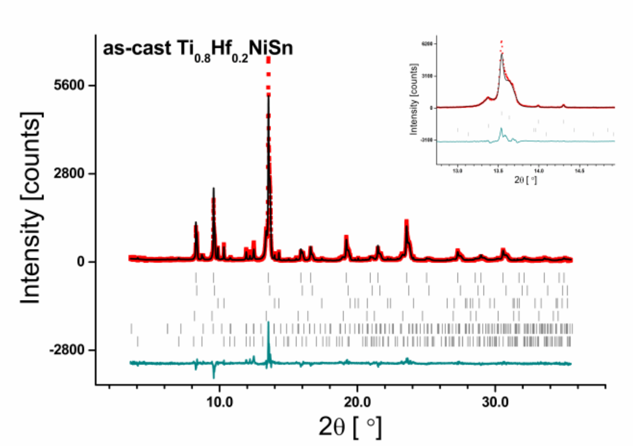

Figure S7. Observed (red), calculated (black) and difference (blue) diffraction profiles collected for as-cast $Ti_{0.8}Hf_{0.2}NiSn$, λ = 0.50218 Å, χ^2 = 2.99. Vertical bars indicate Bragg peak positions of contributing phases, from top to bottom: HH_2, HH_1, Sn, FH, Sn_5Ti_6 and Sn_3Ti_5. Inset shows (220) reflections of the HH and FH phases.

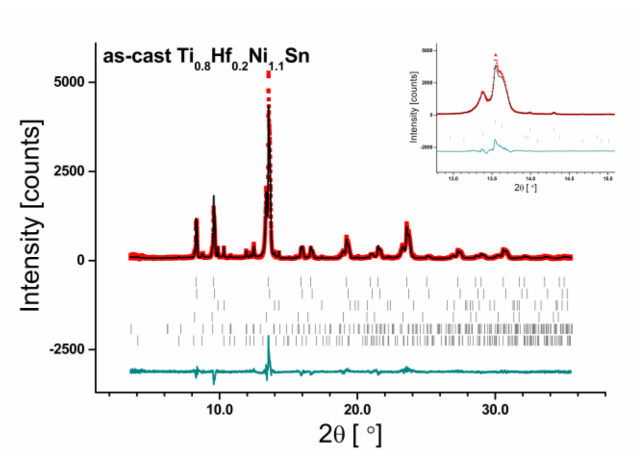

Figure S8. Observed (red), calculated (black) and difference (blue) diffraction profiles collected for as-cast $Ti_{0.8}Hf_{0.2}Ni_{1.1}Sn$, λ = 0.50218 Å, χ^2 = 2.45. Vertical bars indicate Bragg peak positions of contributing phases, from top to bottom HH_2, HH_1, Sn, $TiNi_2Sn$, Sn_5Ti_6 and Sn_3Ti_5. Inset shows (220) reflections of the HH and FH phases.

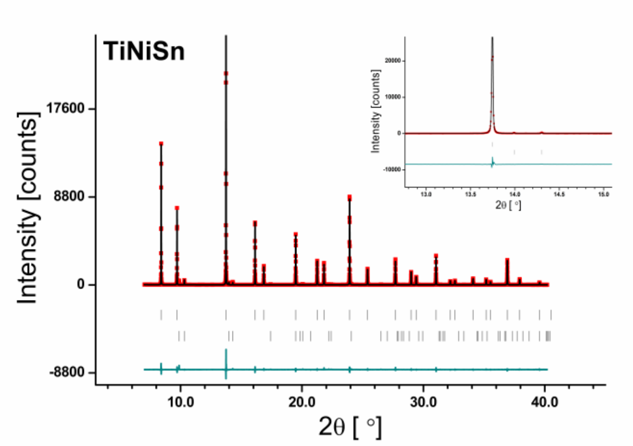

Figure S9. Observed (red), calculated (black) and difference (blue) diffraction profiles collected for annealed TiNiSn, λ = 0.50218 Å, χ^2 = 2.69. Vertical bars indicate Bragg peak positions of contributing phases, from top to bottom: HH and Sn. Inset shows (220) reflections of the HH phase.

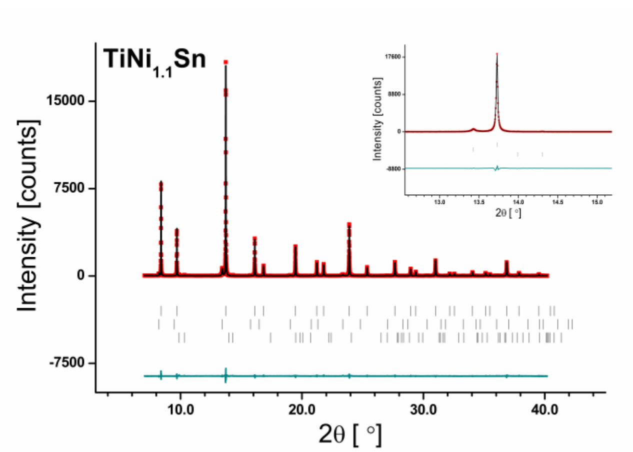

Figure S10. Observed (red), calculated (black) and difference (blue) diffraction profiles collected for annealed $TiNi_{1.1}Sn$, λ = 0.50218 Å, χ^2 = 1.56. Vertical bars indicate Bragg peak positions of contributing phases, from top to bottom: HH, FH and Sn. Inset shows (220) reflections of the HH and FH phases.

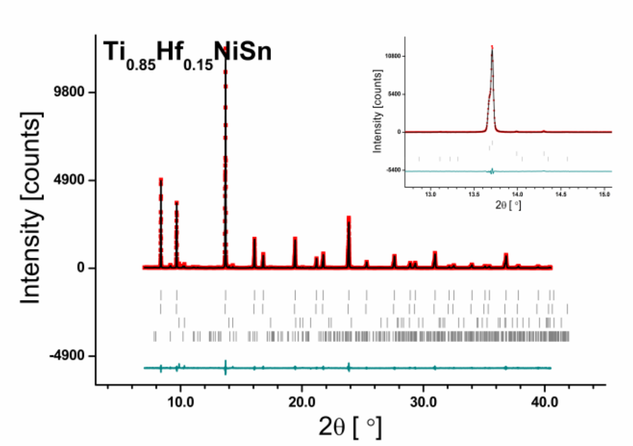

Figure S11. Observed (red), calculated (black) and difference (blue) diffraction profiles collected for ennealed $Ti_{0.85}Hf_{0.15}NiSn$, λ = 0.50218 Å, χ^2 = 1.42. Vertical bars indicate Bragg peak positions of contributing phases, from top to bottom: HH_1, HH_2, Sn and HfO_2. Inset shows (220) reflections of the HH phases.

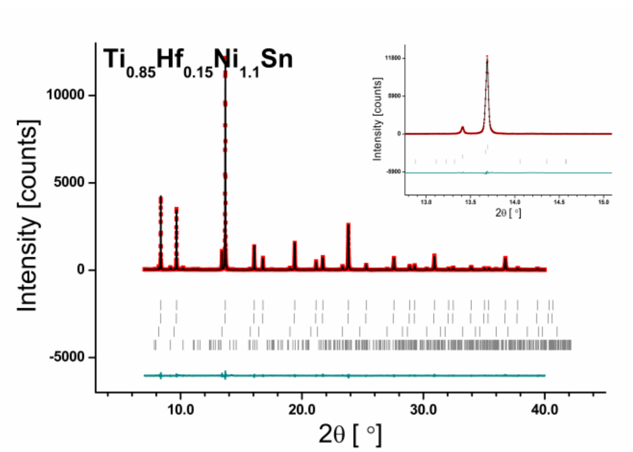

Figure S12. Observed (red), calculated (black) and difference (blue) diffraction profiles collected for annealed $Ti_{0.85}Hf_{0.15}Ni_{1.1}Sn$, λ = 0.50218 Å, χ^2 = 1.22. Vertical bars indicate Bragg peak positions of contributing phases, from top to bottom: HH_1, HH_2, FH and HfO_2. Inset shows (220) reflections of the HH and FH phases.

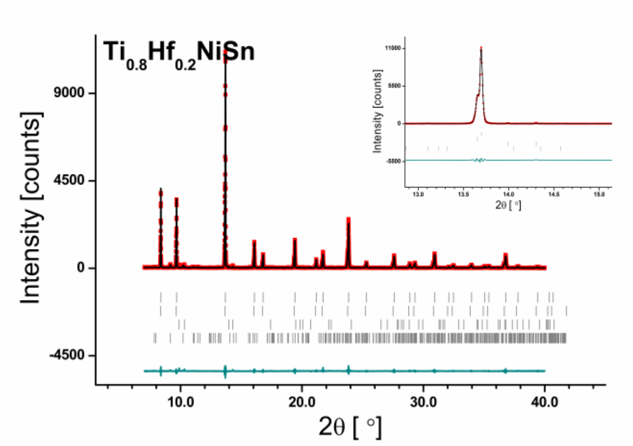

Figure S13. Observed (red), calculated (black) and difference (blue) diffraction profiles collected for annealed $Ti_{0.8}Hf_{0.2}NiSn$, λ = 0.50218 Å, χ^2 = 1.66. Vertical bars indicate Bragg peak positions of contributing phases, from top to bottom: HH_1, HH_2, Sn and HfO_2. Inset shows (220) reflections of the HH phases.

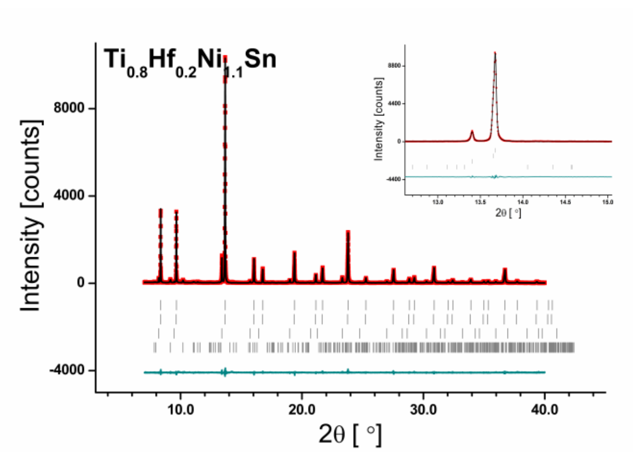

Figure S14. Observed (red), calculated (black) and difference (blue) diffraction profiles collected for annealed $Ti_{0.8}Hf_{0.2}Ni_{1.1}Sn$, λ = 0.50218 Å, χ^2 = 1.17. Vertical bars indicate Bragg peak positions of contributing phases, from top to bottom: HH_1, HH_2, FH and HfO_2. Inset shows (220) reflections of the HH and FH phases.

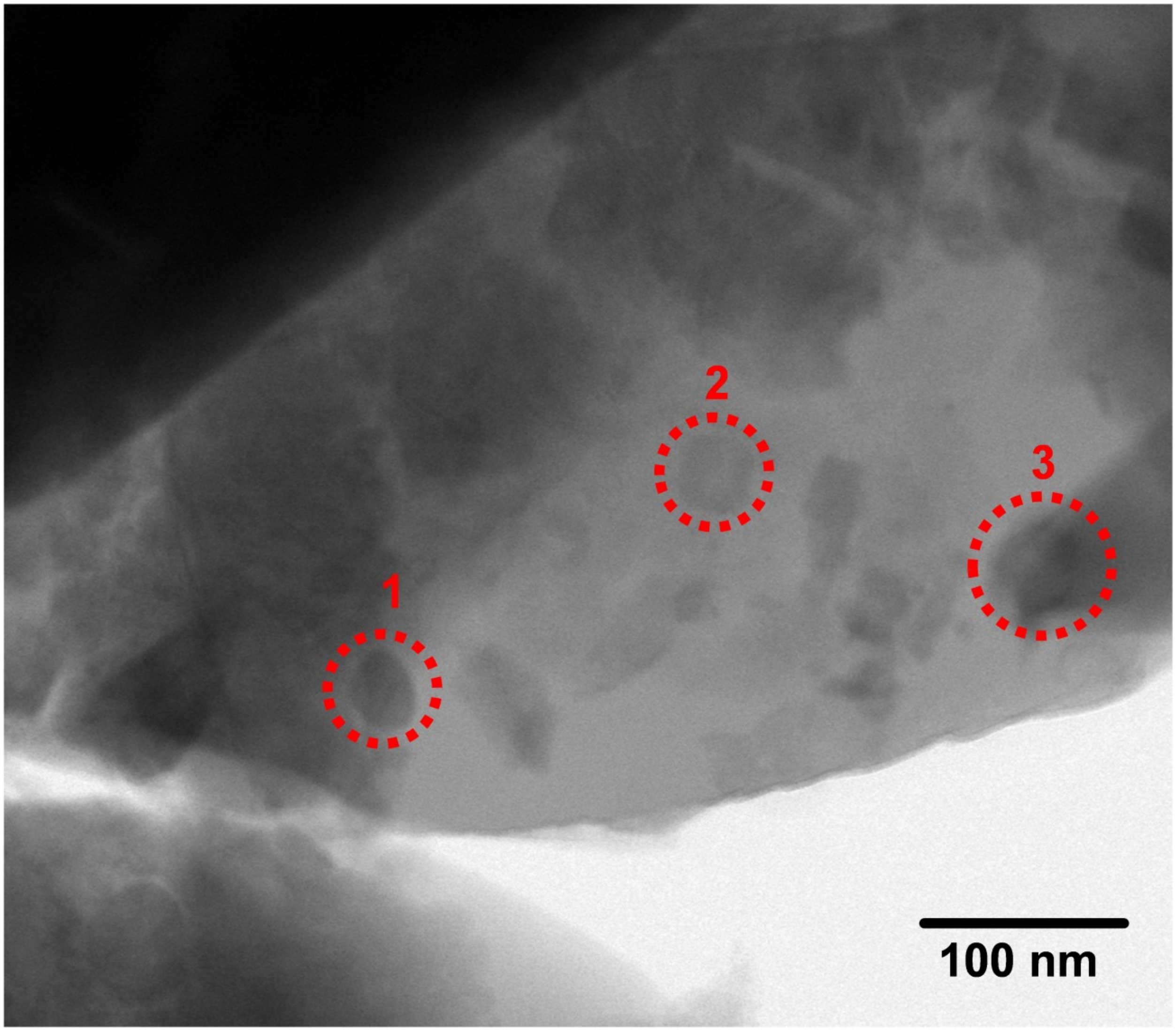

Figure S15. STEM-ABF image of a HH particle with formed precipitates in $Ti_{0.85}Hf_{0.15}NiSn$, 1 – HfO_2, 2 – TiO_2, 3 – TiO_xC_y. The appearing contrast is due to mass-thickness variation among particles.

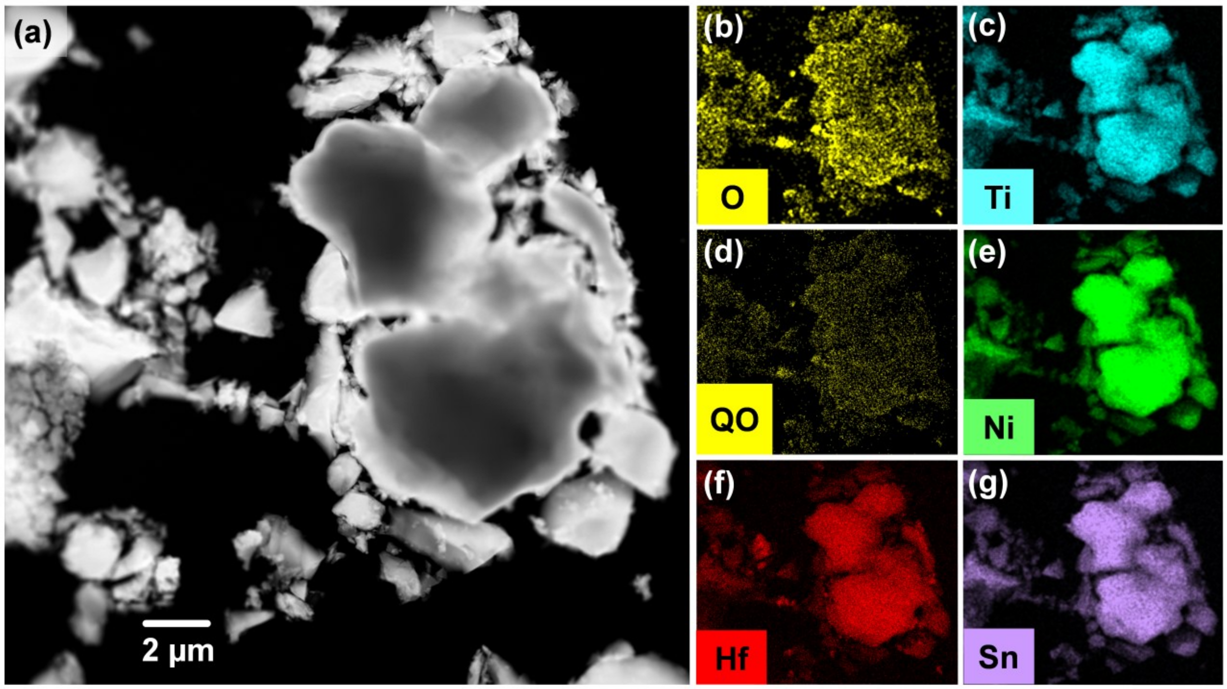

Figure S16. (**a**) STEM-HAADF image of $Ti_{0.85}Hf_{0.15}NiSn$ and corresponding elemental EDS maps (**b–g**) showing a high oxidation degree of the sample material; (**d**) the oxygen EDS quantitative map.

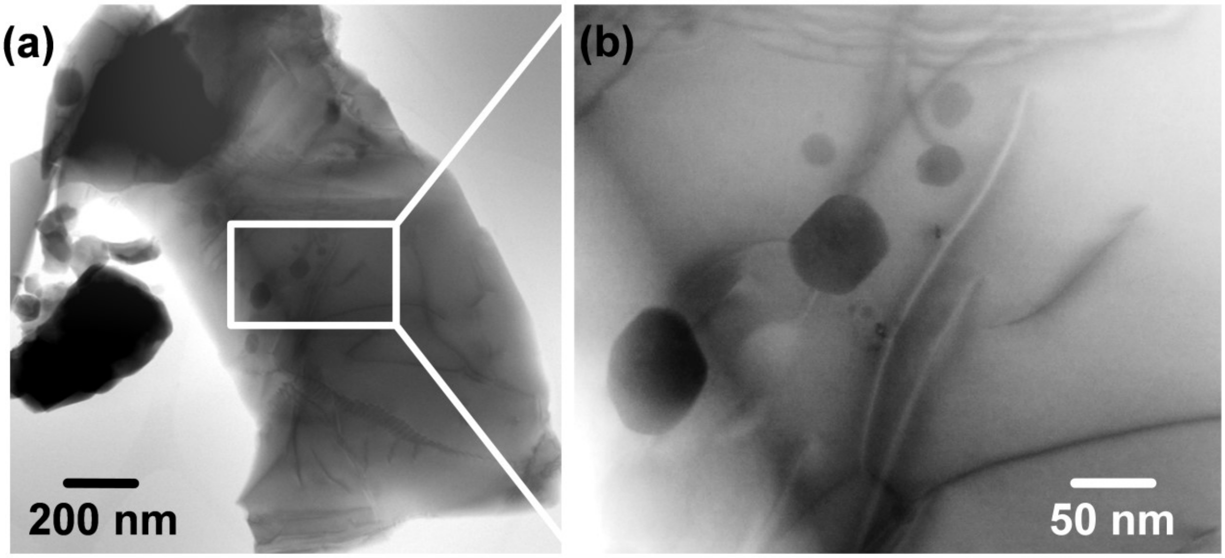

Figure S17. STEM-ABF images of $Ti_{0.8}Hf_{0.2}NiSn$ particles; (**a**) the diffraction contrast emphasizes a high concentration of dislocation networks and HfO_2 nanoprecipitates; (**b**) high magnification STEM-ABF image with the defective HH matrix demonstrating the dislocation pinning effect and the HfO_2 precipitates with varying sizes (10–70 nm).

(a) (b)

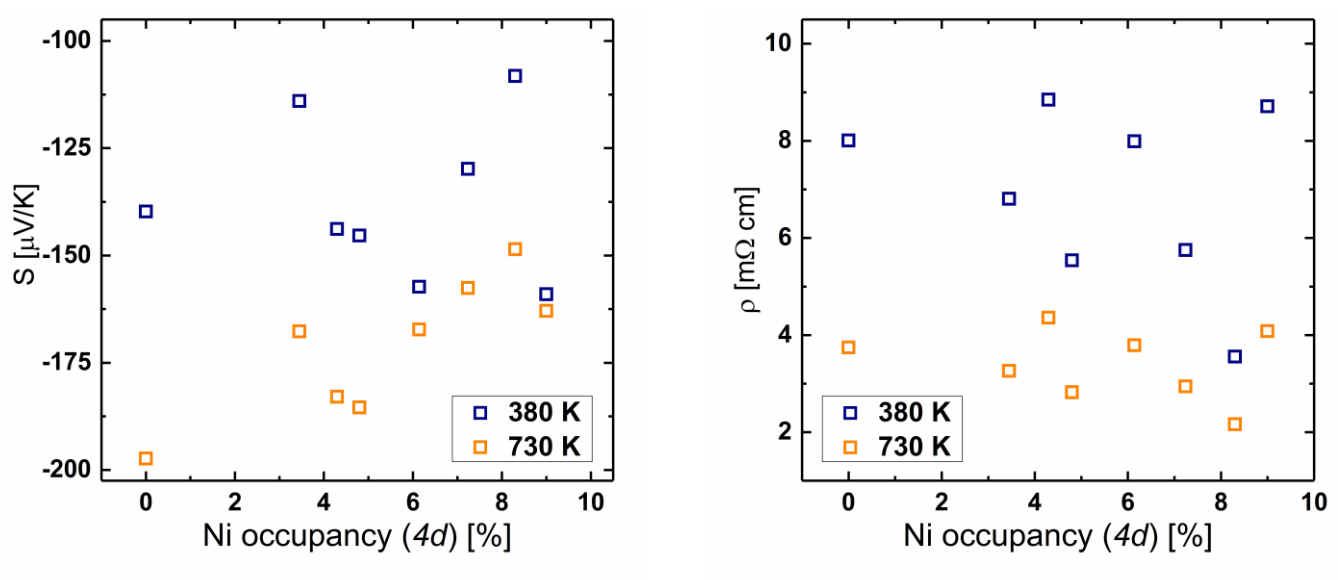

Figure S18. S (**a**) and ρ (**b**) vs. Ni atom occupancy at the *4d* site in all studied HH phases.

(a) (b)

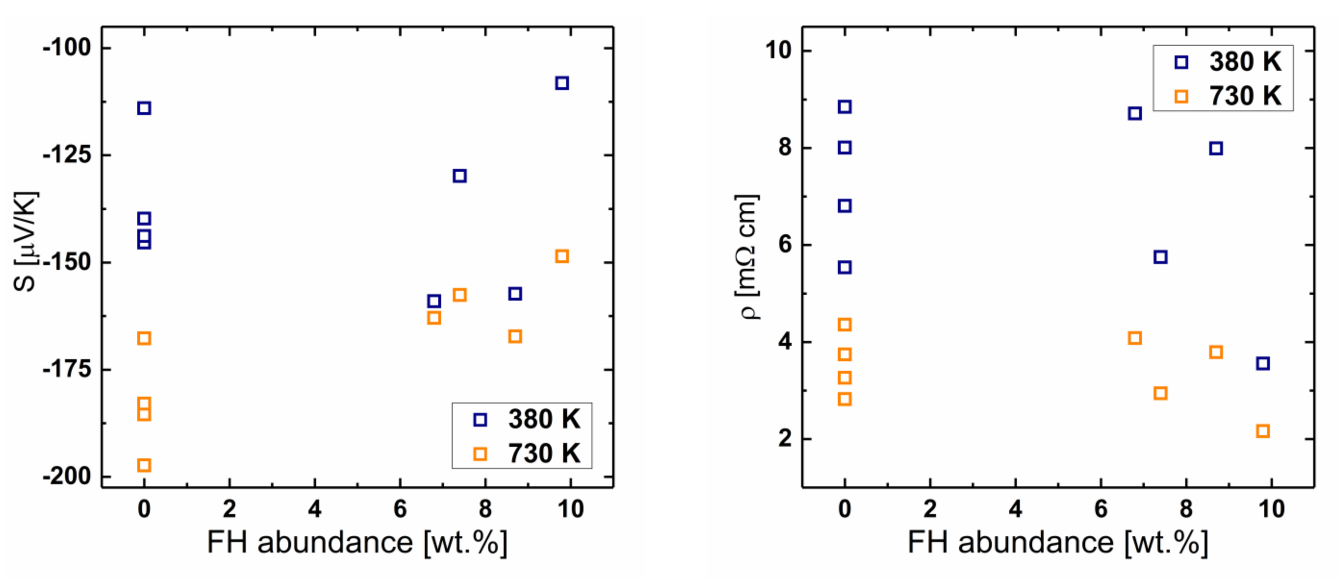

Figure S19. S (**a**) and ρ (**b**) vs. abundance of the FH phase in $Ti_{1-x}Hf_xNi_ySn$ samples.

(a) (b)

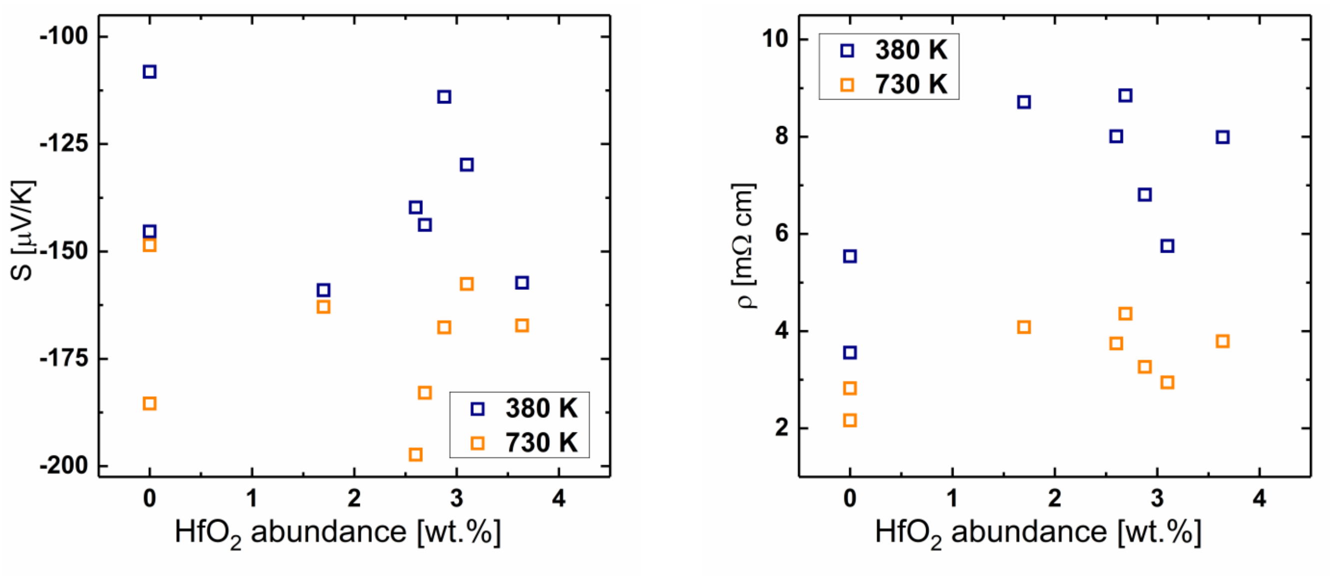

Figure S20. S (**a**) and ρ (**b**) vs. abundance of HfO_2 in $Ti_{1-x}Hf_xNi_ySn$ samples.